

# Comparison of primary glioblastoma Single-cell and Tissue RNA-seq co-expression networks - Submission to PLOS Journals

Brian Arand<sup>2</sup>, Raghu Machiraju<sup>1, 2</sup>, Kun Huang<sup>1, 2</sup>

**1 Department of Biomedical Informatics, The Ohio State University, Columbus, Ohio, The United States of America**

**2 Department of Computer Science and Engineering, The Ohio State University, Columbus, Ohio, The United States of America**

## Abstract

We compare our resulting networks both at the ontology enriched module level and at the gene level...

## Introduction

The isolation of individual cells' transcriptome profiles has been largely a theoretical concept to bioinformaticians. And accordingly, transcriptomic inquiry has been limited to those questions regarding tissues—potentially composed of a heterogeneous hodgepodge of cellular types, subtypes, and states. But with the advent of Single-Cell RNA sequencing (RNASeq) technology, comes the potential for refined resolution in transcriptomic datasets. And expectedly, recent publications suggest a peaking interest in this new landscape of informatics. It has been shown that many bioinformatics techniques that were developed for population-cell tissue samples can be effectively applied to single-cellular datasets. However, co-expression network analysis has largely been an unexplored area of analysis in regards to single-cell RNASeq data. To fill this gap, we leverage this new technology to construct and analyze gene co-expression networks for primary glioblastoma single-cell samples. Glioblastoma is widely known to be a heterogeneous cancer, making it a prime candidate for single-cellular inquiries. For instance, we hypothesized that the averaging of single-cells' profiles within a tissue sample may mask or otherwise confound downstream gene correlations based analysis. Correlation between two genes may exist across tissue samples purely due to changing proportion of cellular subtypes within those samples. However, a single-cellular perspective, of the same tumors may theoretically filter out those artificial tissue-level correlations. And so correlation based analyses, like co-expression network analysis, require study. In our work, we begin this journey by looking at network mining, module detection, and gene enrichment analysis at both the single-cell and population of cell (tissue sample) levels. The final goal of this work is to shed light on the convoluted intricacies of inter-cellular genomic landscape of glioblastoma tissue from a single-cellular perspective.

## Materials and Methods

We analyzed two glioma datasets: GSE57872, the data presented in Single-cell RNA-seq highlights intratumoral heterogeneity in primary glioblastoma [1], and GSE48865, the data presented in RNA-seq of 272 gliomas revealed a novel, recurrent PTPRZ1-MET fusion transcript in secondary glioblastomas [2]. GSE57872 consists of single-cell samples whereas GSE48865 consists of more-traditional, population-of-cell (or tissue) samples. From here on, GSE57872 and GSE48865 samples will be referred to as 'single-cell' and 'population' samples respectively. After preprocessing each dataset independently (details explained in following sections), we step each dataset through a coexpression-network analysis workflow. An overview of this workflow is shown in Fig. 1. Details of and rational for data set dependent variations of this workflow are explained in the sections to follow.

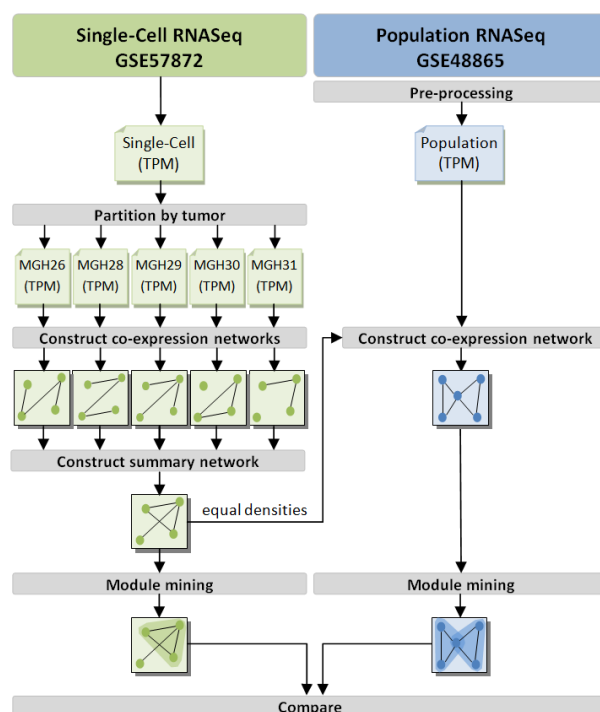


**Figure 1. Network comparison workflow.** Note that there is no partition nor aggregation step in the population RNASeq pipeline. Moreover, note that edges of the constructed population co-expression network are filtered to achieve the closest network density possible to that realized in the Single-Cell pipeline.

## Single-Cell Data

### Single-Cell RNASeq Samples

In this section, we discuss the handling of the GSE57872, single-cell data. This data set is comprised of normalized gene expression values for 5,948 genes for 430 single-cell samples selected by flow cytometry cell sorting and micromanipulation from 5 different primary glioblastomas labeled: MGH26, MGH28, MGH29, MGH30, and MGH31. Patel et al sequenced the cells using SMARTseq protocol [3]. Alignment to hg19 was performed with Bowtie (version 1.1.1) [4] and the authors calculated TPM (transcripts per million) values using RSEM (version 1.2.3) [5]. The final reported values were

log-transformed and mean-shifted per gene. More formally, let  $x_{si}$  be the TPM enrichment value for the  $i^{th}$  gene of sample  $s$ . And let  $N_t$  be the sample size of tumor  $t$ , then the analogous, final reported value,  $y_{si}$ , would be:

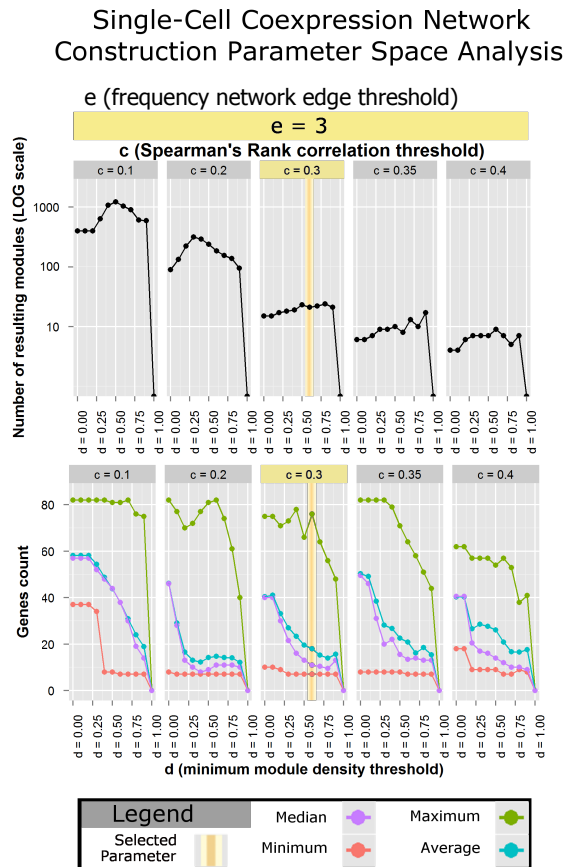


**Figure 2. Parameterization space analysis.** A comparison of module statistics (a) number of modules output (b) distribution statistics of module size in gene count for modules output in one run of CODENSE. Values of the selected parameterization are highlighted in yellow.

$$y_i = \frac{\sum_s \log_2(x_{si} + 1)}{N_t} \quad (1)$$

$$y_{si} = \sum_s \log_2(x_{si} + 1) - y_i \quad (2)$$

### 0.0.1 Network Construction

In our analysis, single-cell samples were grouped by tumor of origin,  $t$ . For each group, a gene-by-gene Spearman's rank correlation matrix was calculated:

$$P_t = \begin{bmatrix} \rho_{11t} & \cdots & \rho_{1kt} \\ \vdots & \ddots & \vdots \\ \rho_{k1t} & \cdots & \rho_{kkt} \end{bmatrix} \quad (3)$$

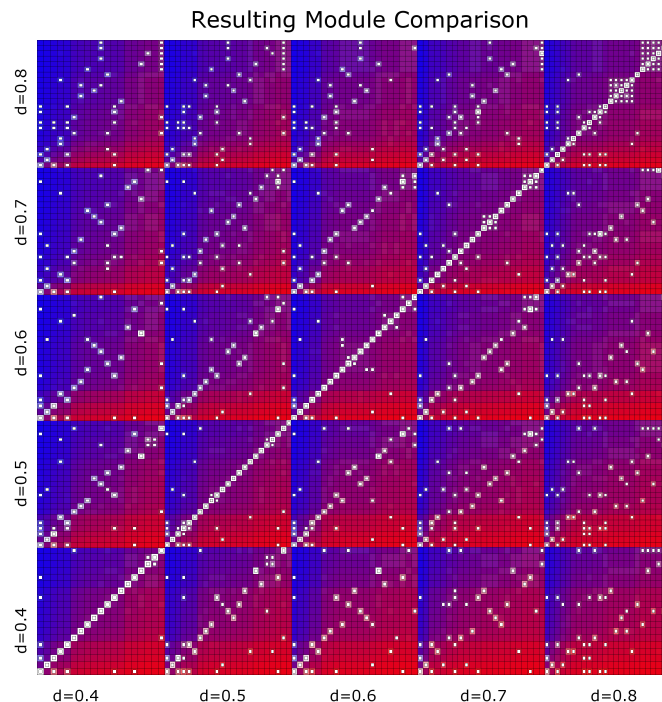


**Figure 3. Parameterization space starry night map.** Here we display the exhaustive gene-set by gene-set enrichment profiles for those modules output by 5 different runs of CODENSE for different values of the minimum density threshold  $d$ . The color of each square encodes the size of some gene set  $A$ , some gene set  $B$ , and the size of  $A \cap B$  relative to  $A \cup B$ . These three values are encoded into the red, blue, and green channels of the square respectively. Thus, the whiter a square is the more similar  $A$  and  $B$  are. Furthermore, a Fisher's exact test was performed for significant enrichment per gene set pair. Placement of a small, white token indicates significant overlap between  $A$  and  $B$ . Note that the central diagonal is all white. Which makes sense because this is the comparison of all sets with themselves. This diagonal pattern is most stable when comparing the selected characterization  $d=0.6$  with each of its neighboring parameterizations than between other neighboring steps shown above

Where  $\rho_{ijt}$  is the Spearman's correlation between the  $i^{th}$  and  $j^{th}$  gene of tumor  $t$ . Co-expression matrices were then created by filtering at the same Spearman's rank threshold,  $c$ , to produce binary matrices,  $B_t$ , per tumor.

$$B_t = \begin{bmatrix} b_{11t} & \dots & b_{1kt} \\ \vdots & \ddots & \vdots \\ b_{k1t} & \dots & b_{kkt} \end{bmatrix}, b_{ijt} = \begin{cases} 1, & |\rho_{ijt}| \geq c \\ 0, & o.w. \end{cases} \quad (4)$$

This is analogous to cutting a co-expression network at a given edge threshold. After analyzing the distribution of resulting networks' densities we settled on a threshold of 0.3 with an associated frequency network density of 0.04. We point out that this threshold is low, but we argue that it is a necessary trade-off given the distribution of correlations. It is expected to see such non-concordant data, because current single-cell RNASeq technology is known to produce noisy data (need a reference for this regarding PCR amplification of single cell).

The binary matrices were then aggregated into a single frequency matrix,  $F$ . This aggregation is performed in an attempt to attenuate patient-specific signals and focus, rather, on glioblastoma-specific patterns of gene co-expression.

$$F = \begin{bmatrix} \sum_t b_{11t} & \dots & \sum_t b_{1kt} \\ \vdots & \ddots & \vdots \\ \sum_t b_{k1t} & \dots & \sum_t b_{kkt} \end{bmatrix} \quad (5)$$

## 0.0.2 Module Detection

It is this matrix  $F$  that is fed into the CODENSE software to be converted into a summary network,  $S$ , and then mined for high-density modules [6].

$$S = (V, E), \text{ where } v_i, v_j \in V \text{ and } (v_i, v_j) \in E \leftrightarrow f_{ij} \geq e \quad (6)$$

Frequency threshold threshold  $e$  was set to be 3 meaning that in order for a given edge representing a gene-gene correlation to appear in the final summary network  $S$ , that same pair of genes had to appear in a majority of the individual  $B_t$  networks.

CODENSE then reported the modules that meet some minimum density threshold,  $d$ . At the suggestion of the CODENSE authors and after analyzing the effect perturbing  $d$  has on the number and size of the resulting modules, we chose a minimum density threshold of 0.6. We wanted to maximize  $d$  to ensure dense modules to ensure their biological significance. Note that in Fig. 2, heightened values of  $d$  can drastically affect the output number and size of modules. Our selection of  $d = 0.6$  marks the upper limit of where this non-robust behavior starts in our selected parameter space sampling resolution. At the selected parameterization, CODENSE reported 21 dense, first-order modules. These relatively high thresholds guarantee that our resulting modules will be dense and therefore will capture only the strongest signals found in the data.

## CODENSE Parameterization Validation

We make a considerable effort to ensure that the resulting modules output by CODENSE at the selected parameterization are robust to change withing the algorithm's parameterization space. Fig. 2 shows that the size and number of output modules are relatively stable at the selected values for  $e$ ,  $c$ , and  $d$  (highlighted in yellow). Furthermore, 3 is a custom visualization we developed to compare set-by-set co-enrichment. The central diagonal is visualized all in white, indicating that the sets compared with themselves all did not change the gene membership of the sets much.

## 0.1 Population Tissue Samples

Our population-tissue control comes from GEO accession GSE48865. 274 glioma tissue samples make up this dataset, of which, 59 were identified as primary, stage-4 glioblastoma tissue samples. We filtered out any reads from the 59 samples with more than 10% of its nucleotides designated as unknown bases, and any read with more than 50% of its bases having Sanger phred+33 quality scores less than 5. After filtering, we retained 1,388,064,773 reads in total.

Each filtered sample was then aligned to hg19 transcriptome (GRCh37) using bow-tie (version 1.1.1 with default parameters provided by RSEM) and TPM values per gene were estimated using RSEM (version 1.2.3). 73% of the reads were aligned successfully either uniquely or multi-mapped. TPM values were adjusted again as in equation 2. Genes were then filtered to retain only those that were highly expressed across the 59 samples. The  $i^{th}$  gene was filtered out if  $y_i \leq 4.5$ . We retained 6,932

genes after filtering, 3,927 of which had also been retained in the analogous steps of the single-cell workflow as illustrated in Fig. ??.

### 0.1.1 Network Construction and Module Detection

Again, as in equation 3, Spearman's Rank correlation was calculated for all genes pair-wise. The Spearman's Rank threshold,  $c$ , from equation 4, was set to 0.02 so as to achieve the same density as the single-cell network. No further network aggregation step was required for this data set.

Modules were also found using the CODENSE algorithm using the same parameterization used in the single-cell workflow described above.

## 0.2 Enrichment

Module sets derived from both the single-cell network and population tissue sample network were then ontology enriched. Modules were enriched for all terms in Gene Ontology Consortium's biological process (BP), cellular component (CC), and molecular function (MF) human ontologies using the David Bioinformatics Resources (version 6.7) Functional Annotation Tool [7]. The most significant (in terms of bonferroni adjusted p-value) ontology per category was reported for each module.

## Results

Using the parameters described above, our workflow produced 21 modules for the single-cell data and 48 modules for the population data set. A breakdown of these modules labeled with their most significant biological process ontology, cellular component ontology, and molecular function ontology is shown for the single-cell data in fig. 4 and for the population data in fig. 5.

Module		Enriched Subset				
ID	Gene Count	Top Ontology	Gene Count	%	PValue	Bonferroni
20	76	BP transport	14	21.88	1.30E-02	1.00E+00
		CC NONE	-	-	-	-
		MF Ras GTPase activator activity	3	4.69	2.87E-02	9.96E-01
3	49	BP translational elongation	42	85.71	7.82E-90	3.09E-87
		CC ribosome	42	85.71	5.28E-75	2.74E-73
		MF structural constituent of ribosome	40	81.63	5.20E-73	3.22E-71
12	42	BP NONE	-	-	-	-
		CC NONE	-	-	-	-
		MF NONE	-	-	-	-
13	26	BP cellular component biogenesis	5	21.74	5.54E-03	9.05E-01
		CC NONE	-	-	-	-
		MF NONE	-	-	-	-
15	26	BP nuclear division	15	57.69	1.25E-19	4.99E-17
		CC spindle	11	42.31	1.07E-15	1.01E-13
		MF ATP binding	11	42.31	6.76E-05	6.43E-03
10	14	BP glycolysis	3	23.08	4.80E-04	2.08E-02
		CC extracellular region part	5	38.46	4.41E-03	3.04E-01
		MF protein binding	10	76.92	1.96E-02	8.62E-01
7	13	BP nervous system development	6	50.00	4.89E-04	2.64E-01
		CC cell fraction	4	33.33	3.44E-02	1.96E-01
		MF transporter activity	6	50.00	8.46E-04	1.14E-01
11	12	BP regulation of Ras protein signal transduction	2	20.00	5.82E-02	1.00E+00
		CC NONE	-	-	-	-
		MF ATPase activity, coupled to transmembrane movement of substances	2	20.00	2.85E-02	9.12E-01
1	11	BP oxidative phosphorylation	4	36.36	3.76E-05	7.56E-03
		CC mitochondrial inner membrane	6	54.55	5.94E-07	3.92E-05
		MF hydrogen ion transmembrane transporter activity	4	36.36	1.66E-05	8.90E-04
2	11	BP glycolysis	4	36.36	1.91E-06	4.36E-04
		CC NONE	-	-	-	-
		MF NONE	-	-	-	-

Module		Enriched Subset				
ID	Gene Count	Top Ontology	Gene Count	%	PValue	Bonferroni
5	11	BP response to DNA damage stimulus	3	27.27	1.34E-02	9.65E-01
		CC nuclear lumen	5	45.45	5.95E-03	2.45E-01
		MF NONE	-	-	-	-
6	11	BP anti-apoptosis	3	27.27	7.13E-03	8.78E-01
		CC extracellular region	6	54.55	2.60E-03	1.77E-01
		MF protein binding	9	81.82	3.31E-02	7.73E-01
9	11	BP nervous system development	4	36.36	2.70E-02	9.98E-01
		CC microtubule	3	27.27	1.21E-02	5.31E-01
		MF protein binding	7	63.64	9.18E-02	9.96E-01
16	10	BP translational elongation	5	55.56	1.69E-02	4.56E-05
		CC cytosolic ribosome	5	55.56	4.30E-08	2.71E-06
		MF structural constituent of ribosome	5	55.56	9.80E-07	5.34E-05
4	9	BP protein folding	4	50.00	6.54E-05	1.53E-02
		CC endoplasmic reticulum lumen	6	75.00	5.90E-11	4.19E-09
		MF unfolded protein binding	4	50.00	1.46E-05	1.11E-03
8	8	BP response to organic substance	6	75.00	6.61E-06	1.63E-03
		CC synaptosome	2	25.00	2.64E-02	6.29E-01
		MF protein dimerization activity	3	37.50	2.38E-02	7.21E-01
19	8	BP DNA replication	4	50.00	8.07E-05	1.93E-02
		CC nucleolus	4	50.00	3.99E-03	1.44E-01
		MF ATP binding	4	50.00	2.40E-02	8.64E-01
21	8	BP response to inorganic substance	3	37.50	2.04E-03	2.06E-01
		CC cytoplasm	4	50.00	9.74E-02	9.83E-01
		MF copper ion binding	4	50.00	3.11E-06	1.54E-04
14	7	BP cellular amino acid metabolic process	2	33.33	3.18E-02	9.02E-01
		CC NONE	-	-	-	-
		MF NONE	-	-	-	-
17	7	BP anatomical structure development	4	57.14	7.48E-02	1.00E+00
		CC cell fraction	3	42.86	4.03E-02	8.82E-01
		MF NONE	-	-	-	-
18	7	BP antigen processing and presentation of peptide antigen	3	50.00	3.78E-05	9.07E-03
		CC MHC class I protein complex	2	33.33	8.77E-03	3.39E-01
		MF MHC class I receptor activity	2	33.33	5.60E-03	1.78E-01

**Figure 4. Single-cell network module ontology enrichment.** A list of the modules output from the CODENSE algorithm ordered by module size, each enriched for BP, CC, and MC ontologies. Row color denotes a certain statistical significance as demarcated in the figure legend.

We compared these output module sets at the module-level and the gene-level. At the module-level, we find that the single-celled modules are enriched for translational

elongation, and many other expected cell cycle and cellular process ontologies such as nuclear division, glycolysis, oxidative phosphorylation, protein folding, and DNA replication. Likewise, we find expected enriched ontologies reported by the population pipeline—namely: translational elongation, cell cycle, extracellular matrix organization, antigen processing, immune response, RNA splicing, and others.

Module		Enriched Subset				
ID	Gene Count	Top Ontology	Gene Count	%	PValue	Benfoni
24	51	BP immune response	18	34.82	6.50E-12	7.91E-09
		CC lysosome	8	15.38	3.50E-06	4.55E-04
37	48	MF Ig binding	3	5.77	2.08E-04	4.08E-02
		BP immune response	14	29.79	5.57E-08	3.63E-05
34	46	CC receptor complex	5	10.64	3.18E-04	3.98E-02
		BP response to external stimulus	14	31.11	1.04E-06	7.68E-04
1	34	CC response to external stimulus	12	26.67	6.83E-12	1.09E-09
		CC lytic vacuole	5	11.11	1.15E-05	6.97E-03
22	34	BP cell cycle	21	63.64	5.07E-19	1.58E-16
		CC nucleus	27	81.82	7.73E-10	8.11E-08
23	31	BP extracellular matrix organization	12	36.36	3.87E-17	1.79E-14
		CC proteinaceous extracellular matrix	19	57.58	2.90E-23	4.20E-21
46	26	MF extracellular matrix structural constituent	13	39.39	6.50E-20	7.48E-18
		BP immune response	12	40.00	1.39E-08	3.17E-06
26	24	CC plasma membrane	18	60.00	3.18E-05	3.55E-03
		MF molecular transducer activity	10	33.33	5.81E-03	5.19E-01
4	21	BP collagen fibril organization	5	20.83	6.80E-08	3.51E-05
		CC extracellular matrix	11	45.45	1.80E-11	2.19E-09
39	17	MF platelet-derived growth factor binding	5	20.83	1.09E-08	1.29E-07
		BP response to external stimulus	12	52.17	1.53E-08	9.49E-06
43	16	CC extracellular region	11	47.83	5.61E-05	5.60E-03
		MF keratogen binding	2	5.70	4.55E-03	4.45E-01
10	15	BP translational elongation	16	80.00	5.54E-32	8.48E-29
		CC ribosome	16	80.00	7.43E-27	3.56E-25
21	15	BP structural constituent of ribosome	16	80.00	1.55E-28	1.51E-26
		CC anatomical structure morphogenesis	9	56.25	1.28E-06	1.14E-03
18	13	CC basal lamina	3	18.75	1.12E-04	1.12E-02
		BP protein binding	16	87.76	1.42E-03	1.54E-01
38	13	CC cell adhesion	7	46.47	1.85E-05	5.13E-03
		BP proteinaceous extracellular matrix	4	26.67	2.49E-03	2.38E-01
11	12	MF extracellular matrix structural constituent	3	20.00	2.78E-03	1.99E-01
		BP none	-	-	-	-
25	12	CC none	-	-	-	-
		MF none	-	-	-	-
13	12	BP establishment of localization in cell	6	42.86	1.55E-04	2.91E-02
		CC endoplasmic reticulum	9	46.29	1.68E-07	1.36E-05
17	12	MF isomerase activity	3	21.43	3.29E-03	2.59E-01
		BP response to external stimulus	6	50.00	1.44E-04	5.91E-02
3	11	CC plasma membrane	6	50.00	3.97E-02	9.38E-01
		MF anion transmembrane transporter activity	2	16.67	9.30E-02	1.00E+00
29	11	BP antigen processing and presentation of peptide or protein antigens via MHC class I	9	75.00	1.60E-20	4.37E-18
		CC MHC class II protein complex	8	66.67	3.65E-18	1.94E-16
40	11	MF MHC class II protein complex	7	58.33	2.46E-16	4.65E-14
		BP none	-	-	-	-
5	10	CC membrane part	7	63.64	5.87E-02	9.11E-01
		MF none	-	-	-	-
11	12	BP synaptic transmission	3	27.27	8.70E-03	8.59E-01
		CC compact myelin	2	18.18	2.24E-03	1.35E-01
13	12	MF structural constituent of myelin sheath	2	18.18	2.97E-03	1.81E-01
		BP nitrogen compound metabolic process	9	81.82	1.80E-06	4.60E-02
17	12	CC macromolecular complex	8	72.73	1.94E-05	5.42E-03
		MF transcription activator activity	5	45.45	5.99E-05	5.67E-03
25	12	BP immune system process	6	50.00	2.04E-04	1.00E-02
		CC neoplastic cell	3	27.27	3.44E-03	1.88E-01
2	11	MF enzyme binding	3	27.27	2.90E-02	9.27E-01
		BP RNA splicing	6	60.00	3.75E-07	4.84E-05
3	11	CC ribonucleoprotein complex	7	70.00	8.65E-08	4.06E-06
		MF RNA binding	7	70.00	8.77E-07	4.38E-05
29	11	BP RNA metabolic process	5	50.00	3.74E-04	1.11E-01
		CC intracellular membrane-bounded organelle	10	100.00	2.01E-01	8.94E-02
40	11	MF RNA binding	3	30.00	6.48E-02	9.79E-01
		BP cell fate commitment	3	30.00	1.96E-03	3.41E-01
5	10	CC none	-	-	-	-
		MF transcription regulator activity	4	40.00	2.56E-02	8.24E-01
29	11	BP response to biotic stimulus	3	30.00	1.85E-02	9.96E-01
		CC endoplasmic reticulum lumen	3	30.00	8.79E-04	7.12E-02
40	11	MF enzyme inhibitor activity	-	-	-	-
		BP none	-	-	-	-
5	10	CC none	-	-	-	-
		MF none	-	-	-	-

**Figure 5. Population network module ontology enrichment.** A list of the modules output from the CODENSE algorithm ordered by module size, each enriched for BP, CC, and MC ontologies. Row color denotes a certain statistical significance as demarcated in the figure legend.

Make note that one of the most significantly enriched ontologies reported for the population pipeline was extracellular matrix organization. Single-cell modules did not enrich for this specific ontology.

We then profiled the two lists of output ontology enriched modules to find both consensus and marginal ontologies between the two data sets. When using exact equality to define the intersection between the two sets of ontologies, we find that only two ontologies were identified by both single-cell and population pipelines. To get a better understanding of the similarities of the pipelines' output, we report what we will be calling 'contextual ontologies' in the intersection. We aim to summarize ontologies reported by both pipelines by seeking close common ancestors within the GO hierarchical database of ontologies. More concretely, a contextual ontology is the root of the shortest possible subtree with height no greater than 2 that connects at least one ontology that was reported by the single-cell pipeline with at least one ontology that was reported by the population pipeline. These contextual ontologies, along with both the marginal and consensus ontologies are reported in fig. 7.



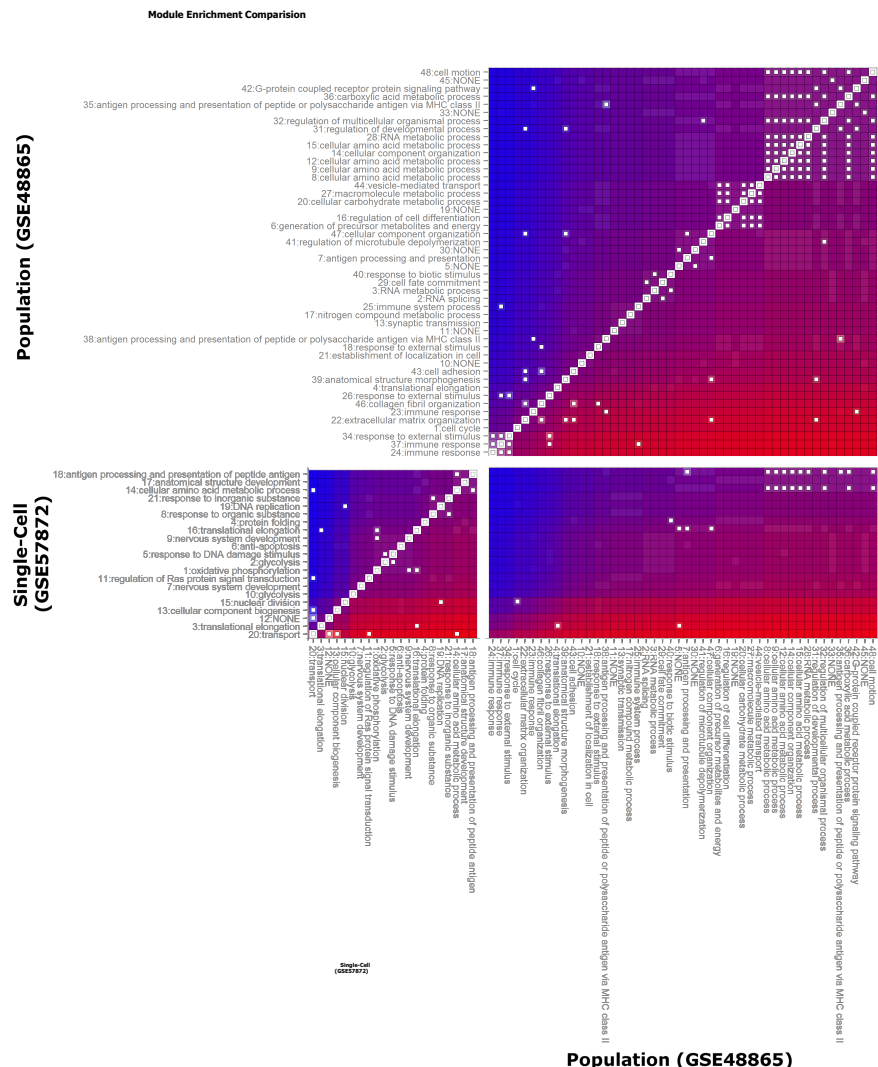


Figure 6. Gene-level starry map comparison of output modules.

## Discussion

Our analysis illustrates the potential of single-cell co-expression network module enrichment analysis as a potential tool for biological inquiry. We find that, when taking the contextual approach to comparing the sets of reported ontologies, most of the more significantly enriched ontologies reported by the population data were related to those reported by single-celled data. The single-celled approach to network module ontology enrichment may also prove to filter out biological signals like extracellular matrix as our results suggest. This may be of particular interest to studies that are specifically interested in intracellular environments rather than entire microenvironments.

## References

1. Patel AP, Tirosh I, Trombetta JJ, Shalek AK, Gillespie SM, Wakimoto H, et al. Single-cell RNA-seq highlights intratumoral heterogeneity in primary glioblastoma.



- Science. 2014;344(6190):1396–1401. Available from:  
<http://www.sciencemag.org/content/344/6190/1396.abstract>.
2. Bao ZS, Chen HM, Yang MY, Zhang CB, Yu K, Ye WL, et al. RNA-seq of 272 gliomas revealed a novel, recurrent PTPRZ1-MET fusion transcript in secondary glioblastomas. *Genome Research*. 2014 Aug;24(11):1765–1773. Available from:  
<http://www.ncbi.nlm.nih.gov/pmc/articles/PMC4216918/>.
3. Ramskold D, Luo S, Wang YC, Li R, Deng Q, Faridani OR, et al. Full-length mRNA-Seq from single-cell levels of RNA and individual circulating tumor cells. *Nat Biotech*. 2012 Aug;30(8):777–782. Available from:  
<http://dx.doi.org/10.1038/nbt.2282>.
4. Langmead B, Trapnell C, Pop M, Salzberg S. Ultrafast and memory-efficient alignment of short DNA sequences to the human genome. *Genome Biology*. 2009;10(3):R25. Available from: <http://genomebiology.com/2009/10/3/R25>.
5. Li B, Dewey C. RSEM: accurate transcript quantification from RNA-Seq data with or without a reference genome. *BMC Bioinformatics*. 2011;12(1):323. Available from: <http://www.biomedcentral.com/1471-2105/12/323>.
6. Hu H, Yan X, Huang Y, Han J, Zhou XJ. Mining coherent dense subgraphs across massive biological networks for functional discovery. *Bioinformatics*. 2005;21(suppl 1):i213–i221. Available from: [http://bioinformatics.oxfordjournals.org/content/21/suppl\\_1/i213.abstract](http://bioinformatics.oxfordjournals.org/content/21/suppl_1/i213.abstract).
7. Huang DW, Sherman BT, Lempicki RA. Systematic and integrative analysis of large gene lists using DAVID bioinformatics resources. *Nat Protocols*. 2008 Dec;4(1):44–57. Available from: <http://dx.doi.org/10.1038/nprot.2008.211>.

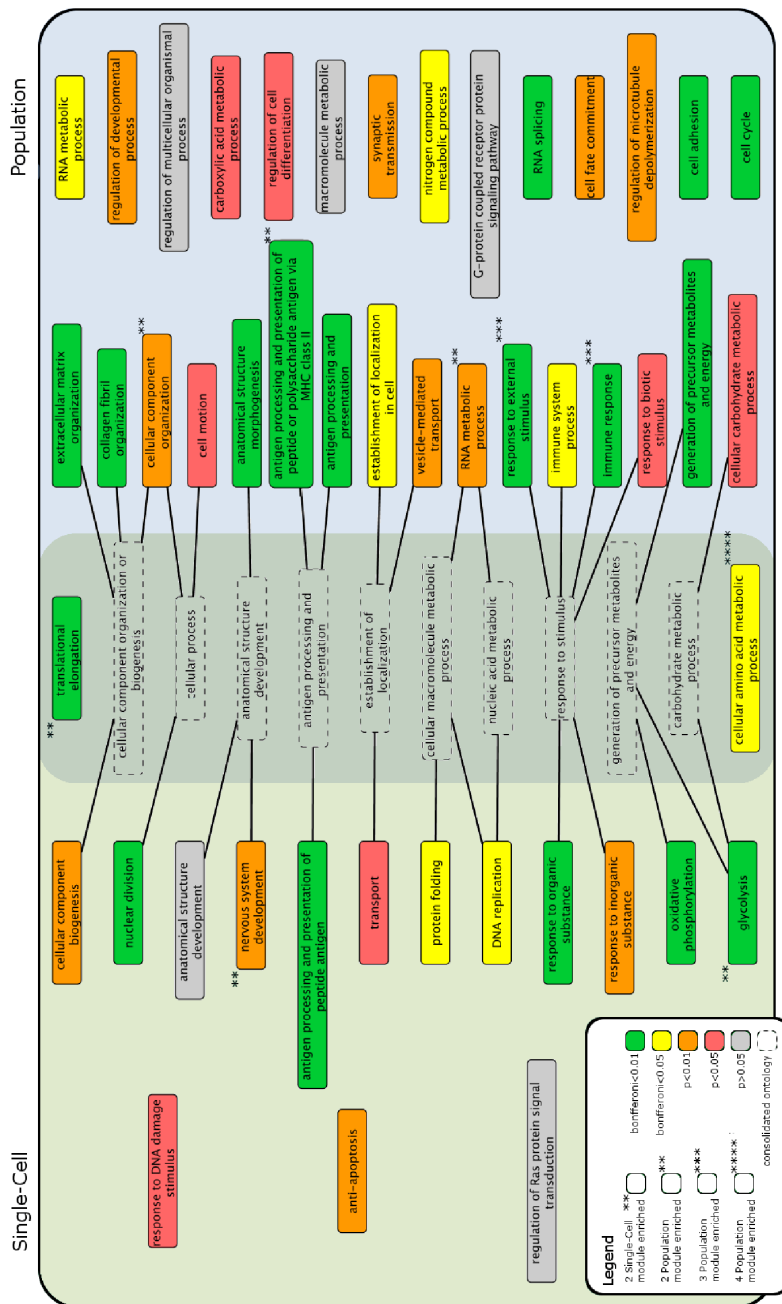


**Figure 7. Enriched module comparison**